BIOCHEMISTRY
including biophysical chemistry & molecular biology
Article

Biochemistry **2010,** *49,* 1533–1540 1533
DOI: 10.1021/bi901753h

The Clustering and Spatial Arrangement of β-Sheet Sequence, but Not Order, Govern α-Synuclein Fibrillogenesis†

Jae-Eun Suk,‡ Sowmya Bekshe Lokappa,‡ and Tobias S. Ulmer*

Department of Biochemistry and Molecular Biology and Zilkha Neurogenetic Institute, Keck School of Medicine, University of Southern California, 1501 San Pablo Street, Los Angeles, California 90033. ‡These authors contributed equally to this work.

Received October 11, 2009; Revised Manuscript Received December 29, 2009

ABSTRACT: The intrinsically unstructured protein α-synuclein (aS) is prone to misfold into cytotoxic β-sheet-rich oligomers and amyloid fibrils that underlie the pathogenesis of Lewy body diseases such as Parkinson's disease. An important, recognized fibrillogenesis parameter is amino acid content, whereas the influence of amino acid sequence distribution is not as well understood. The fibril core of aS encompasses five regions of high β-sheet propensity, termed β1−β5. Using four aS variants with identical amino acid compositions but rearranged pseudorepeat motifs, we show that β2−β5 sequence clustering, but not order, is important for efficient fibrillogenesis. For molecular species progressing toward the fibrillar state, order invariably increases; i.e., the spatial arrangement of sequence elements becomes restricted. By introducing disulfide bonds in a fibril structure-based manner, we demonstrated that a successful protofibril-to-fibril conversion is dependent upon the spatial arrangement of sequence elements of high β-sheet propensity. Moreover, a disulfide-linked aS dimer is shown to fibrillize rapidly. We propose that a conformational search underlies the emergence of a fibrillar aS nucleus that is directed by gaps in sequence between β-sheet regions and the accessible range of spatial β-sheet arrangements in soluble, prefibrillar oligomers. On the basis of the universal cross-β-sheet structure of amyloid fibrils, these principles are expected to apply to a wide range of amyloidogenic proteins.

In the course of the past century, there has been a significant improvement in the recognition and prevalence of pathological conditions associated with improper protein deposition in humans (*1*, *2*), perhaps in correlation with increased life expectancies. Pathological proteinaceous deposits have been associated with a number of diseases, most notably the prevalent neurodegenerative disorders (*3*−*5*). Protein deposits implicated in dementia are rich in predominantly one of three proteins (α-synuclein, β-amyloid, and tau), all of which are intrinsically unstructured but nevertheless deposited as ordered fibrils (*3*−*7*). Consequently, an undesired folding pathway can be populated by these proteins, which leads to conversion of soluble monomeric proteins into insoluble amyloid fibrils. This pathway involves the formation of small oligomers (dimers, trimers, etc.) that assemble into soluble protofibrils, which eventually make the transition into insoluble fibrils (*4*−*7*). The structures of all examined amyloid fibrils contain a core region of cross-β-sheet structure, and soluble oligomers generally exhibit a significant content of β-sheet structure (*4*, *7*, *8*). This suggests that interactions between β-sheet-rich protein conformations give rise to the initiation, maturation, and propagation of fibrillar misfolding in a rather universal manner. It has even been proposed that such self-propagating proteins, capable of storing information in a particular β-sheet arrangement, represented the first functioning biomolecules (*9*).

The misfolding of α-synuclein (aS)[1] has been implicated in the demise of dopamineric neurons of the *substantia nigra*, which is associated with the phenotype of Parkinson's disease (*5*, *10*). The sequence of the 140-residue protein aS comprises seven 11-residue degenerate repeats succeeded by a tail of low hydrophobicity and high net charge (Figure 1A and Figure S5 of the Supporting Information). The pseudorepeat sequence has amphiphilic character (Figure 1A,B), reminiscent of apolipoproteins (*11*), and allows aS to reversibly bind synaptic vesicles (*11*, *12*), which, in turn, may inhibit neurotransmission (*13*). Within small variations between aS fibril preparations, deposited aS fibrils exhibit a rigid core encompassing residues 37−95 (*14*−*17*), which implicates the amphiphilic pseudorepeat sequence in misfolding. Within this sequence, which places aS outside of the typical charge−hydrophobicity phase space of intrinsically unfolded proteins (*18*), a 35-residue segment (residues 61−95), termed the NAC (non-Aβ-amyloid component) region, had early on been implicated in neurodegeneration (*19*). An isolated peptide corresponding to the NAC region is capable of fibrillizing (*20*). However, aS fibrillogenesis is modulated by interactions that involve virtually its entire sequence and can even be abrogated despite the presence of the NAC sequence (*21*−*25*). Thus, while distinct sequence motifs are important for fibrillogenesis, they can be context-dependent. It was further shown that protein mean charge, mean hydrophobicity, and mean β-sheet propensity allow fibrillization predictions of considerable accuracy for many proteins, including wild-type aS and mutant forms

†Support from The John Douglas French Alzheimer's Foundation, the American Heart Association, and the National Institutes of Health (HL089726) is gratefully acknowledged.

*To whom correspondence should be addressed. E-mail: tulmer@usc.edu. Telephone: (323) 442-4326. Fax: (323) 442-4404.

[1]Abbreviations: aS, α-synuclein; bS, β-synuclein; NAC, non-Aβ-amyloid component; SaS, sequence-rearranged α-synuclein.

Published on Web 01/25/2010

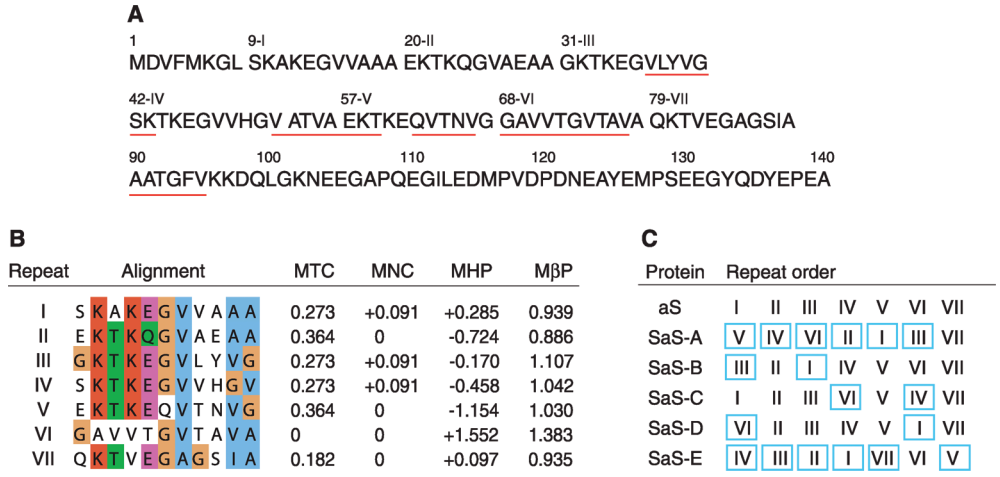

FIGURE 1: Amino acid sequence of human α-synuclein and designed sequence-rearranged variants. (A) Sequence of wild-type aS. Residues 37−43, 52−59, 62−66, 68−77, and 90−95, which have been reported to form β-strands in aS fibrils (*15*), are underlined. (B) Sequence alignment of the seven 11-residue aS pseudorepeats. Conserved amino acids are colored by the Jalview multiple-alignment editor (*56*) using the ClustalX color scheme. The mean total charge (MTC), mean net charge (MNC), mean hydrophobicity (MHP), and mean β-sheet propensity (MβP) are listed. Values were calculated as described in the literature (*22*), but employing the Kyte−Doolittle hydrophobicity scale (*57*). (C) Repeat order of the pseudorepeat-swapped aS variants (SaS). Swapped repeats are shown boxed. The four-residue insert between repeats IV and V [residues 53−56 (A)] is unchanged. Variant SaS-A was examined previously (*32*, *34*) and is listed for the sake of comparison.

incorporating amino acid changes (*22*, *26*). Combining the evaluation of such features in computational approaches that often consider β-sheet pairing possibilities and/or sequence motifs also led to useful predictions about the fibrillization propensity of amino acid sequences (*27*−*31*). In contrast to the amino acid content and certain sequence motifs, the influence of the amino acid sequence distribution and the role of the spatial arrangement of sequence elements on fibrillogenesis are not as well understood and are the focus of this study.

The influence of amino acid sequence distribution can be examined by studying sequence-rearranged aS variants. An additional advantage of studying such variants is that a constant amino acid content is maintained; i.e., mean physicochemical properties are kept identical to those of the wild type. A recent study of this nature revealed that an aS sequence rearrangement based on interactions with several aggregation-inhibiting small molecules can abolish fibrillogenesis in apparent correlation to the fragmentation of β-sheet sequence propensities (*32*). We examine the general significance of this observation here in more detail by studying four specific rearrangements of aS pseudorepeats to evaluate the effects of β-sheet sequence clustering and order on fibrillogenesis. The progression of a molecular species along the fibrillization pathway invariably leads to an increase in its structural definition; an aS molecule transitions from a monomeric, unfolded state to the fibrillar, folded state, where it contributes to nucleating a fibril core or joins an existing cross-β-sheet arrangement. The structural determinants that govern the transitions between the defined higher-order aggregates (e.g., the protofibril-to-fibril transitions) are unknown. To gain further insight into the mechanism of pathological aS misfolding, we examined six engineered intra- or intermolecular disulfide-mediated sequence restrictions that were based on the aS fibril structure (*15*), thereby enabling us to study the influence of β-sheet spatial arrangement on fibrillogenesis.

EXPERIMENTAL PROCEDURES

Molecular Biology and Protein Production. The genes of four aS variants with shuffled pseudorepeats, termed SaS-B−E (Figure 1C and Figure S1 of the Supporting Information), were assembled from overlapping synthetic oligonucleotides by PCR (*33*) and were subcloned into the pET44 expression vector (Novagen, Inc.). Six disulfide-restricted variants were generated by altering selected codons in the wild-type aS expressing pRK172 vector to encode cysteine, using QuikChange mutagenesis (Stratagene, Inc.). One variant incorporated an intermolecular disulfide bond at residue A11, termed aS(11)−aS(11), and one variant incorporated an intramolecular disulfide bond between A11C and V26C, termed aS(11−26). Four variants incorporated an intramolecular disulfide bond that pairs T81C with V63C, T64C, N65C, and V66C, termed aS(63−81), aS(64−81), aS(65−81), and aS(66−81), respectively.

For all variants as well as wild-type aS and β-synuclein (bS), overexpression in *Escherichia coli* and protein purification were performed as described previously for the wild type (*32*, *34*). However, variants containing cysteines were lysed by heat shock under reducing conditions (10 mM β-mercaptoethanol, 1 mM EDTA, and N_2 atmosphere). Prior to protein purification, disulfide bond formation was allowed to take place via dialysis of the reducing agent overnight at 4 °C. This resulted in a range of disulfide-linked aS oligomers. To obtain the desired disulfide-linked monomeric or dimeric protein species (intra- or intermolecular linkage), we separated the covalently linked oligomers by gel filtration (Figure S2 of the Supporting Information), employing a Sephacryl S100HR 26/60 column (GE Healthcare, Inc.). Electrospray mass spectrometry confirmed the expected mass of the disulfide-linked variants (Table 1), and sample purity is illustrated by SDS−PAGE (Figure S2 of the Supporting Information).

Fibrillization Kinetics, Electron Microscopy, and CD Spectroscopy. Thioflavin T fluorescence was monitored to measure the emergence of amyloid fibrils as a function of time (*35*, *36*). To remove previously formed aggregates, protein solutions were passed through a 100 kDa cutoff filter (Sartorius Stedim Biotech GmbH) immediately prior to use. This resulted in the absence of protofibrils and fibrils as evidenced by electron microscopy (Figure S3 of the Supporting Information). In the absence of fibrils that are capable of directly seeding new

Table 1: Electrospray Mass Spectrometry of Disulfide-Restricted aS Variants[a]

aS variant	expected mass (Da)	measured mass (Da)
aS(11)−aS(11)	28982.4	28985
aS(11−26)	14494.2	14495
aS(63−81)	14464.2	14464
aS(64−81)	14462.2	14462
aS(65−81)	14449.2	14450
aS(66−81)	14464.2	14465

[a]An accuracy of 0.01% of the expected mass may be anticipated for electrospray mass spectrometry.

fibrils (*37*), thioflavin T fluorescence monitors the emergence of amyloid fibrils (*35*, *36*) from the monomeric 14 kDa proteins and any potential residual amount of small oligomers. However, when using aS protein preparations of different ages, few differences in fibrillization kinetics were found (Figure S4 of the Supporting Information), suggesting that the amount of residual small oligomers was constant and/or small.

A thioflavin T (Calbiochem, Inc.) stock solution was prepared at 5 mM in Milli-Q H_2O and filtered through a 0.2 μm cellulose acetate filter. Protein fibrillogenesis was evaluated at a protein concentration of 100 μM in 25 mM NaH_2PO_4/Na_2HPO_4 (pH 7.4), 0.02% NaN_3 solution. Samples were incubated at 37 °C in upright 1.5 mL Eppendorf tubes under circular agitation (3 mm stroke, 1200 rpm), using an Eppendorf Thermomixer. Thioflavin T fluorescence was measured at selected time points (Figures 3 and 5B) via removal of a constant volume from the incubated sample, dilution with a 50 mM glycine·NaOH solution (pH 8.5), and addition of thioflavin T to yield final concentrations of 5 μM protein and 25 μM thioflavin T. We immediately took fluorescence measurements on a Varian Cary Eclipse fluorimeter by exciting the samples at 446 nm (5 nm slit width) and scanning the emission wavelength from 450 to 550 nm (20 nm slit width). Fluorescence intensities at 482 nm were plotted as a function of time after subtraction of the buffer signal and fitted to a sigmoidal function.

For electron microscopy, 10 μL of the incubated sample was taken after 168 h, placed on carbon-coated copper grids (Electron Microscopy Sciences, Inc.) for 10 min, and stained with 2% uranyl acetate for 1 min. Images were taken on a Jeol JEM 1400 electron microscope operated at 100 kV. CD measurements were taken at 25 °C on a JASCO J-810 spectropolarimeter using the 100 kDa cutoff filtered protein (20 μM) in a 10 mM KH_2PO_4/K_2HPO_4 solution (pH 7.4). For each sample, eight scans were accumulated, averaged, and corrected for the buffer signal.

RESULTS

Role of β-Sheet Sequence Clustering and Order in aS Fibrillogenesis. On the basis of backbone amide proton H−D exchange and secondary $^{13}C^{\alpha}-^{13}C^{\beta}$ chemical shifts, five β-strands, $\beta1-\beta5$, encompassing residues 37−43, 52−59, 62−66, 68−77, and 90−95, respectively (Figure 1A), were recently assigned to the aS fibril core (*15*). Overall, these definitions are in good agreement with the β-sheet propensities of the aS sequence (Figure 2A), and we use $\beta1-\beta5$ to denote both β-sheet propensities and actual β-sheet structure. Furthermore, intramolecular $\beta1-\beta2$, $\beta2-\beta3$, $\beta3-\beta4$, and $\beta4-\beta5$ interactions were postulated to contribute to the formation of five layers of parallel, in-register $\beta1-\beta1'-\beta1''$, $\beta2-\beta2'-\beta2''$, etc., sheets among aS, aS′, and aS″ molecules to form cross-β-sheet structure (*15*). To assess the importance of the clustering and the order of strands $\beta1-\beta5$ in the context of an unaltered aS amino acid composition (mean physicochemical properties), four sequence-rearranged aS variants, termed SaS-B, -C, -D, and -E, were prepared (Figure 1C). Although a number of rearrangement schemes may have been envisioned, we restricted ourselves to the swap of the 11-residue aS pseudorepeats (Figure 1B). In addition to producing changes in β-sheet propensity distributions (Figure 2), this concomitantly altered the distribution of charges and hydrophobicities (Figure 1B,C and Figure S5 of the Supporting Information).

Variant SaS-B exchanged repeat III at the beginning of the fibril core with repeat I outside of the core (Figure 1C) to reduce β-sheet clustering (Figure 2A,B). Nevertheless, fibrillization was

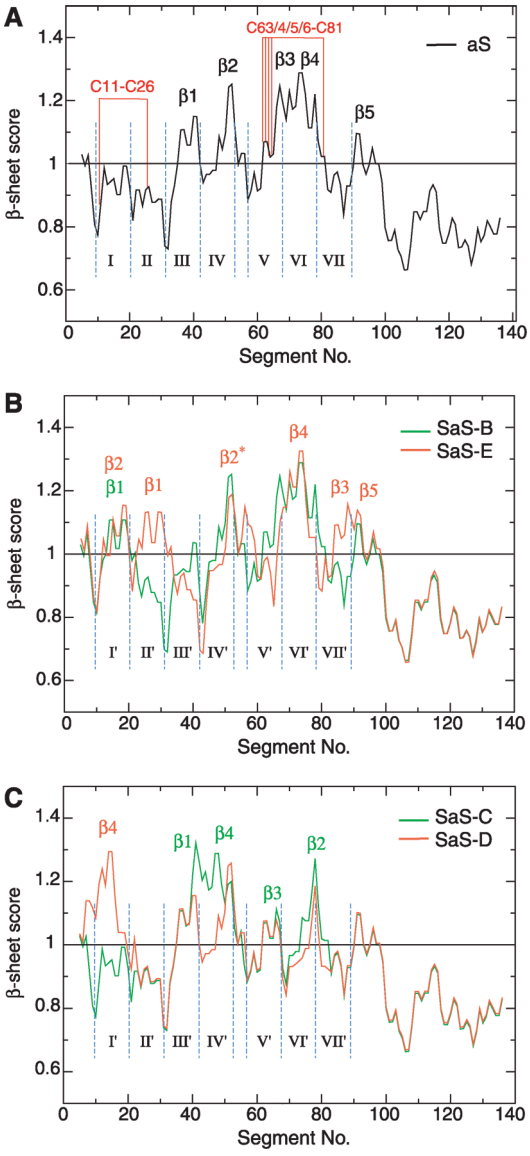

FIGURE 2: β-Sheet propensity distributions of wild-type aS and sequence-rearranged variants. The tabulated β-sheet propensity of each amino acid residue (*58*) is averaged over a nine-residue segment and is denoted by its center residue. Segments are shifted along the sequence by one-residue increments. (A) For wild-type aS, five regions of high β-sheet propensity, termed $\beta1-\beta5$, are marked. The patterns of disulfide-restricted aS variants are highlighted in red. Roman numerals denote the pseudorepeat order. (B and C) For variants SaS-B−E, the rearranged $\beta1-\beta5$ regions are labeled. In SaS-E, a newly formed region of high β-sheet score at the wild type's $\beta2$ region is denoted $\beta2$*. Rearranged pseudorepeats are marked as I′−VII′.

similar to that of wild-type aS with a somewhat longer lag time (Figures 3 and 4A,B), indicating that fibrillogenesis proceeded without $\beta1-\beta2$ sequence proximity and perhaps also without $\beta1-\beta1'$ cross-β-sheet interactions. Variant SaS-C, which has swapped repeats VI and IV (Figure 1A,C), failed to fibrillize under the same conditions (Figure 3). It resulted in the deposition of amorphous aggregates, as evidenced by a comparison to β-synuclein (bS) aggregates (Figure 4D,E). bS is nonamyloidogenic and exclusively forms amorphous aggregates (*32*, *38*, *39*). This indicated that the canonical aS fibrillization pathway had been disturbed. Despite SaS-C having incurred only one repeat swap, β-sheet pairing possibilities, as well as hydrophobic and electrostatic sequence patterns, were significantly altered throughout $\beta1-\beta4$ (Figure 2C and Figure S5 of the Supporting Information). As a result, a new β-sheet and hydrophobic cluster comprised of $\beta1$ and $\beta4$ was created at the expense of mainly $\beta3$.

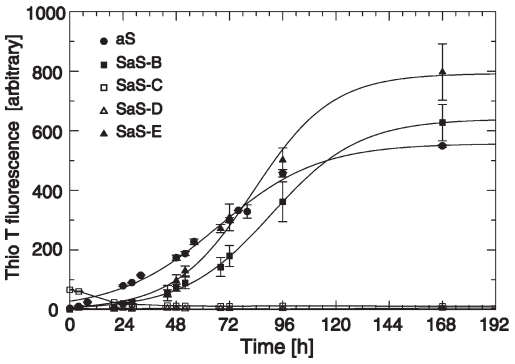

FIGURE 3: SaS fibrillization kinetics. Emergence of amyloid fibrils as a function of time, monitored by observation of thioflavin T fluorescence (*35*, *36*). For fibrillizing variants, the initial lag in fibrillization corresponds to the nucleation phase and the exponential curve to fibril growth. The mean intensities and standard errors were calculated from three independent experiments.

The decrease in the $\beta3$-sheet score in the context of the new sequence environment effectively increased the gaps between the $\beta1/\beta4$ and $\beta2$ regions compared to that of the wild type, resulting in the fragmentation of regions of high β-sheet propensity. Interestingly, the new $\beta1/\beta4$ cluster, which exhibits a comparable β-sheet propensity and increased hydrophobicity compared to those of the $\beta3-\beta4$ region of wild-type aS, was unable to trigger SaS-C fibrillization. In SaS-D, the swap of repeats VI and I transferred $\beta4$ to the N-terminus, which also increased the level of fragmentation of β-sheet propensities (Figures 1C and 2C). Consequently, the absence of fibrillization and deposition of SaS-D as amorphous aggregates (Figures 3 and 4F) was not surprising. An extensive fragmentation of β-sheet propensities compared to that of the wild type had also been noted for the nonfibrillizing variant SaS-A that had been studied earlier (Figure 1B,C and Figure S6 of the Supporting Information) (*32*, *34*). Finally, variant SaS-E implemented three repeat swaps (Figure 1C) that were devised to rearrange β-sheet propensities without introducing new gaps, except for $\beta1$ (Figure 2B). On the basis of the fibrillizing nature of SaS-B, $\beta1$ β-sheet propensities were allowed to be dispersed. The SaS-E sequence configuration, which preserved the distribution of hydrophobicity and charge well relative to those of wild-type aS (Figure S5 of the Supporting Information), readily fibrillized with, again, a lag time somewhat longer than that of the wild type (Figures 3 and 4C). In conclusion, within the context of unchanged mean physicochemical molecular properties, fibrillizing SaS-B and SaS-E shows promiscuity and redundancy in wild-type aS β-sheet sequence order and pairings, whereas SaS-C, SaS-D, and SaS-A signify a limited tolerance for gaps in sequence between regions of high β-sheet propensity and perhaps hydrophobicity as well.

Role of β-Sheet Spatial Arrangement in aS Fibrillogenesis. In the course of aS misfolding, a dimeric species is detectable (*32*, *40*), suggesting that certain interactions between members of the dynamically unfolded aS structural ensemble

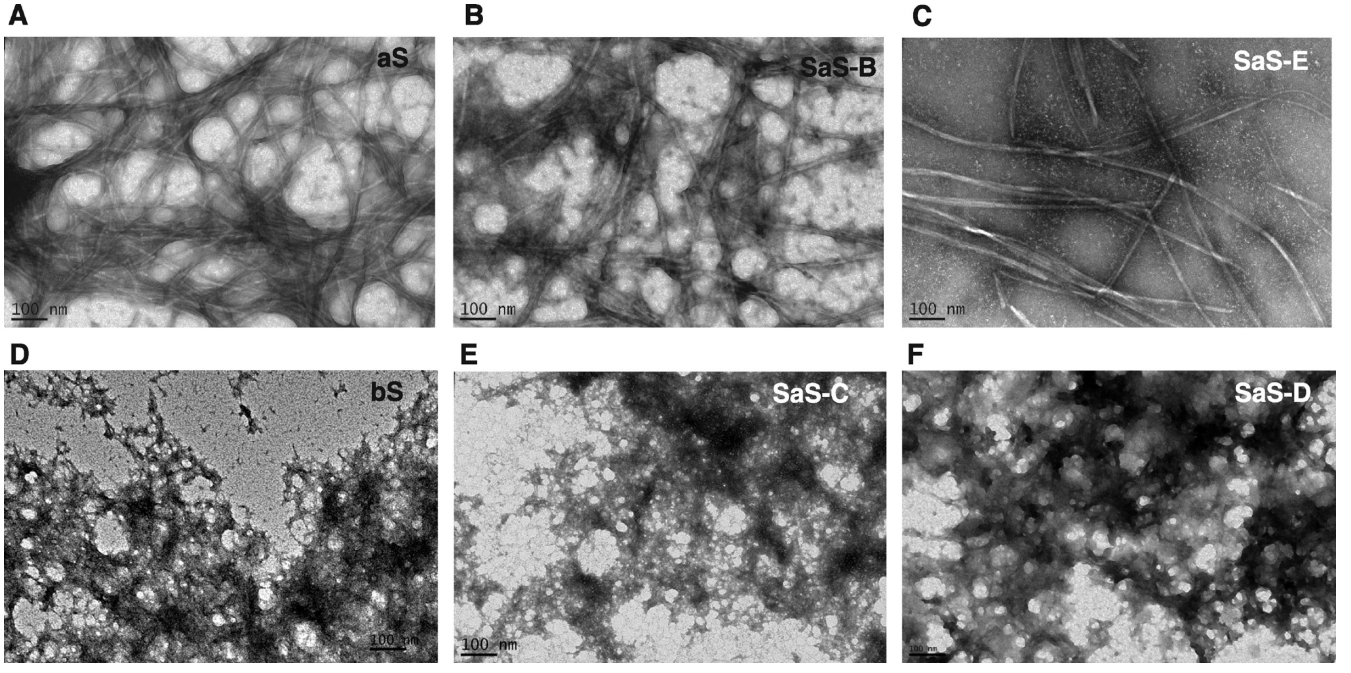

FIGURE 4: Morphology of SaS aggregates as visualized by electron microscopy. For reference, the ordered, fibrillar and disordered, amorphous aggregate morphologies of amyloidogenic aS and nonamyloidogenic bS are shown in panels A and D, respectively. (B and C) The morphology of SaS-B and SaS-E aggregates is fibrillar. (E and F) In contrast, SaS-C and SaS-D were deposited as amorphous aggregates. All aggregates were observed after incubation for 168 h. The scale bar is 100 nm.

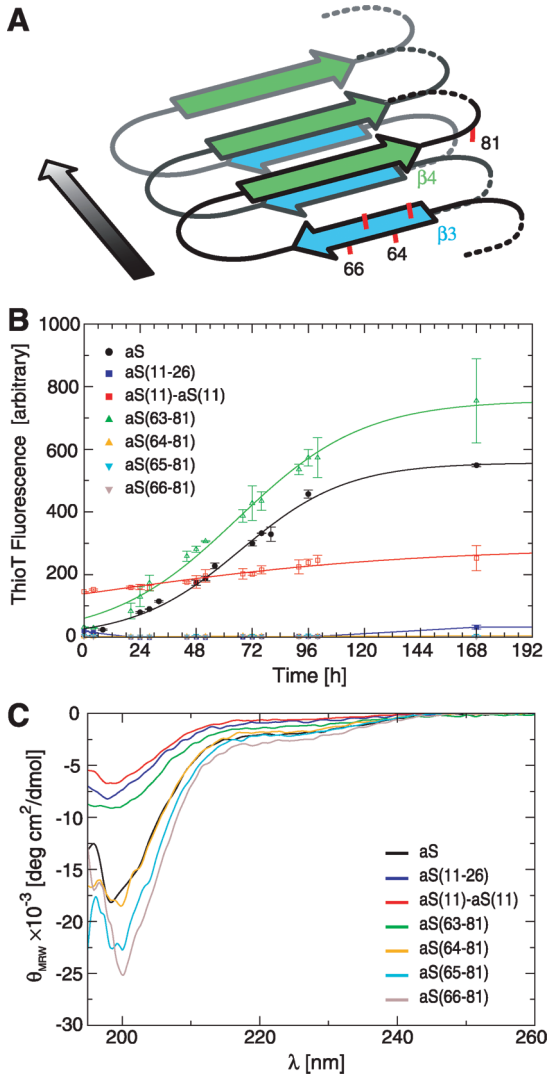

FIGURE 5: Disulfide-restricted aS fibrillization kinetics and structural ensemble preferences. (A) Model of the $\beta3-\beta4$ arrangement in the aS fibril (*15*). (B) Emergence of amyloid fibrils as a function of time, monitored via observation of thioflavin T fluorescence (*35*, *36*). The mean intensities and standard errors were calculated from three independent experiments. (C) CD spectra of disulfide-restricted aS variants in comparison to that of the wild type. Ellipticities are reported as mean residue ellipticity.

(*41*, *42*) can give rise to such a misfolded species, which may be viewed as the first step of the fibrillization pathway. Similarly, the transition to higher-order structures (e.g., the protofibril-to-fibril transition) may depend on the accessible structures of constituent molecules, most notably β-sheet arrangements, since aS amyloid fibril formation results in defined cross-β-sheet structure (*14*, *15*, *17*). Here, we investigated whether transitions to higher-order oligomers can be favored, or disfavored, upon restriction of β-sheet spatial arrangements in a fibril structure-based manner. To bias the structural ensemble of aS, disulfide bonds can be introduced (*43*). This approach was employed to restrict the aS structural ensemble around the region of highest predicted β-sheet propensity, encompassing strands $\beta3$ and $\beta4$ (Figure 2A). We prepared four disulfide-restricted variants by pairing T81C, located in the $\beta4-\beta5$ connector, with V63C, T64C, N65C, and V66C of strand $\beta3$ (Figure 5A), termed aS(63−81), aS(64−81), aS(65−81), and aS(66−81), respectively. Since the side chains of two consecutive residues of a β-sheet point in opposite directions, at most two of the four disulfide variants were expected to efficiently fibrillize into the canonical cross-β-sheet arrangement of wild-type aS. Moreover, the closer the disulfide pairings become in sequence, the more disturbances in intramolecular $\beta3-\beta4$ stacking would ensue (Figure 5A). This would lead to a less compact fibril core, unless compensated by additional rearrangements involving $\beta1$, $\beta2$, and $\beta5$. For comparison, the A11C−V26C pairing, termed aS(11−26), outside of the fibril core was studied (Figure 2A). Moreover, A11C was used to generate a disulfide-linked dimer, termed aS(11)−aS(11), which may accelerate the sampling of intermolecular interactions leading to aS misfolding. It is noted that all amino acid substitutions did not change the aS charge distributions and altered amino acid hydrophobicities and β-sheet propensities in a conservative manner.

As expected, not all T81-paired variants fibrillized (Figure 5B); only aS(63−81) produced fibrils (Figures 5B and 6A). For aS(64−81), aS(65−81), and aS(66−81), the predominantly observed species were protofibrils (Figure 6B−D), showing that the protofibril-to-fibril transition was blocked, whereas initial β-sheet assembly was sufficiently efficient to largely prevent unspecific, amorphous aggregation (Figure 7). We also note that aS(63−81) and aS(66−81) have substituted the same residue types (valine and threonine), thus excluding any difference in misfolding behavior due to a change in mean protein physicochemical properties. The permissive range of β-sheet spatial arrangements in protofibrils therefore appears larger than in fibrils. The aS(11−26) variant unexpectedly produced fibrils very slowly despite its cysteine pairing outside of the fibril core (Figures 2A, 5B, and 6E), allowing a dominant amount of amorphous aggregation to occur (Figures 5B and 6E). Apparently, its initial oligomerization was relatively inefficient (Figure 7). As expected, the aS(11)−aS(11) dimer fibrillized rapidly. In addition to more "conventional" elongated fibrils, it also produced small linear and dense spherical particles (Figure 6F). The lack of any significant fibrillization lag time (Figure 5B) suggested that aS(11)−aS(11) was able to rapidly initiate the formation of molecular species along the fibrillization pathway. Intermolecular disulfide-linked aS avoids the entropic penalty of dimer formation (from monomeric aS) and increases the local aS concentration, accelerating the rate of aS−aS encounters. In conclusion, the ability of aS(64−81), aS(65−81), and aS(66−81) to form protofibrils but, unlike aS(63−81), not fibrils demonstrates that a successful protofibril-to-fibril conversion is dependent upon the accessible spatial arrangement of sequence elements of high β-sheet propensity.

Finally, we may expect that the introduced spatial restrictions affected the ensemble of dynamically unstructured protein conformations. The far-UV CD spectra of aS(64−81), aS(65−81), and aS(66−81) were similar to those of wild-type aS, but those of aS(11−26), aS(63−81), and aS(11)−aS(11) were shifted toward more positive mean ellipticities (Figure 5C). Although all CD spectra were characteristic of proteins exhibiting dynamically unstructured ensembles (*44*), this difference, which is present at all wavelengths, indicated a shift in underlying ensemble conformer distributions relative to the wild type. It would be compatible with an increase in "extended" protein backbone conformations [ellipticity increase at 198 nm (Figure 5C)]. Albeit interesting to note, these observations are nevertheless difficult to interpret in terms of fibrillization propensity because only aS(63−81) and aS(11)−aS(11), but not aS(11−26), fibrillized efficiently.

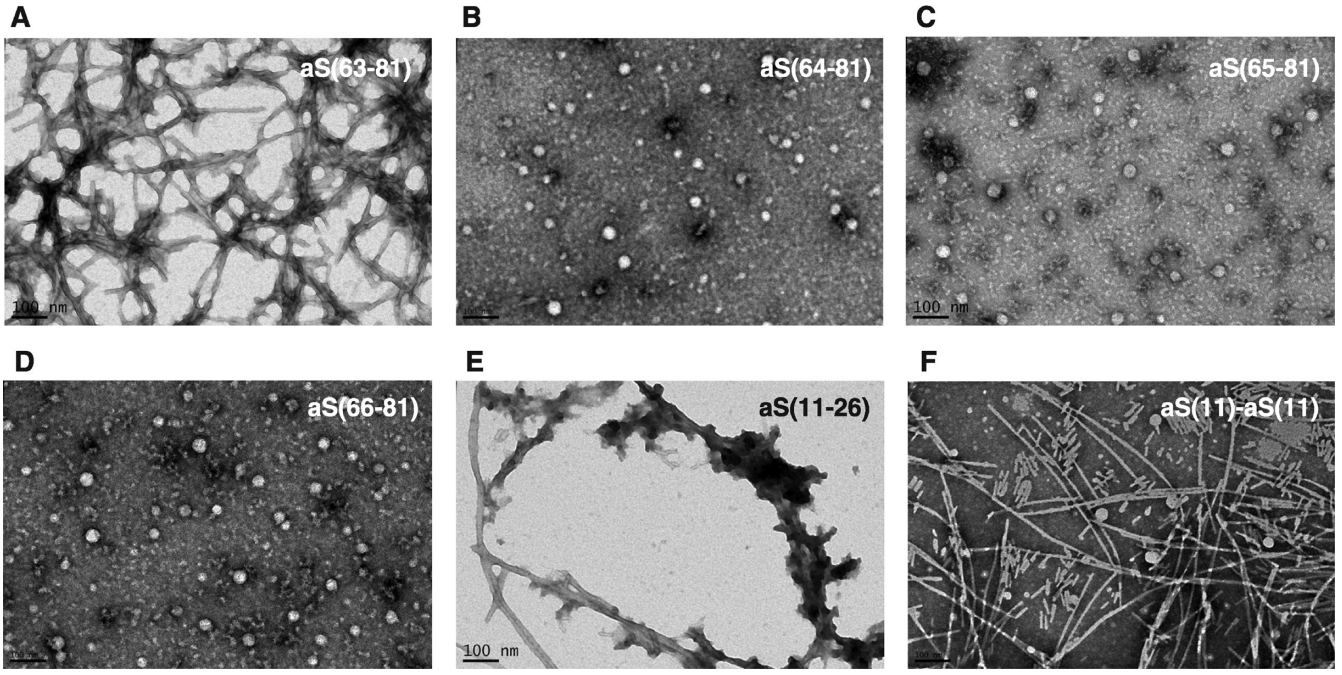

FIGURE 6: Morphology of disulfide-restricted aS aggregates as visualized by electron microscopy. (A−D) Morphology of aS(63−81), aS(64−81), aS(65−81), and aS(66−81) aggregates, respectively. Fibrils were observable for aS(63−81), whereas for the other variants, the presence of protofibrils and the absence of fibrils are evident. (E) Examples of encountered aS(11−26) fibrils, despite the deposits being predominantly amorphous in nature. (F) Morphology of aS(11)−aS(11) fibrils. Extended fibrils were dominant, but small linear and dense spherical particles were also encountered. All aggregates were observed after incubation for 168 h. The scale bar is 100 nm.

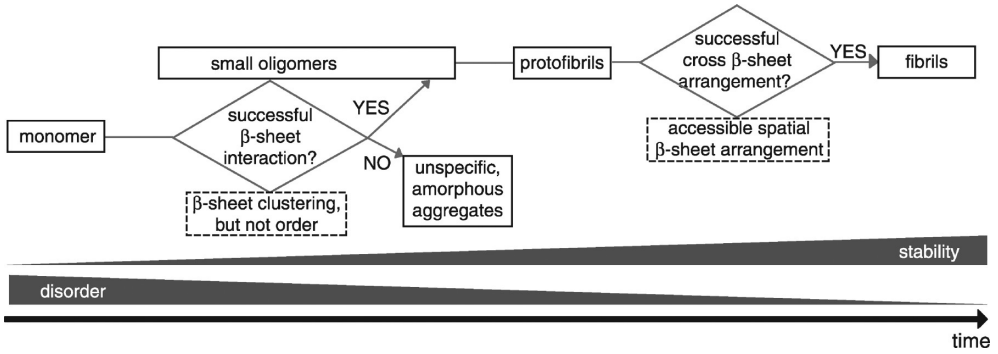

FIGURE 7: Hypothetical flow diagram of the aS conformational search for a fibril-nucleating species. The identified criteria for advancing on the fibrillar pathway are shown in dashed boxes. A range of small oligomers may be formed, not all of which may be competent to form protofibrils.

DISCUSSION

Central to developing therapeutic approaches aimed at neutralizing the pathological species formed along the fibrillar misfolding pathway (*3*, *4*, *6*, *7*) is a detailed understanding of the fibrillar aggregation mechanism. By analyzing the fibrillization kinetics and morphologies of four sequence-rearranged aS variants with identical mean physicochemical properties, we have shown that fibrillogenesis is tolerant to the order of sequence elements of high β-sheet propensity, but not to their fragmentation. In other words, cross-β-sheet pairings and intramolecular β-sheet stacking are promiscuous in aS fibrils. On the basis of the observation of different filament morphologies between aS mutants of differing mean physicochemical properties, it had been noted that multiple molecular interactions can underlie the fibril assembly of aS (*22*). In addition, different fibrillar β-sheet arrangements were observed in wild-type aS and its aS(A53T) variant (*45*). Nevertheless, the extent of the sequence promiscuity revealed in this study is perhaps surprising. In variant SaS-E, 24 of 59 nonequivalent fibril core residue positions were exchanged (Figure S1 of the Supporting Information), but fibrillization was nonetheless highly efficient. In marked contrast, fibrillization kinetics were sensitive to an increase in gaps in sequence between regions of high β-sheet propensity. Considering the elevated β-sheet content of early aS oligomers (*46*, *47*), this suggests that gaps constitute a kinetic barrier to "finding" a fibril-nucleating species before aggregation proceeds in an unspecific, amorphous manner (Figure 7). This is reminiscent of the concentration dependence of formation of either fibrillar or amorphous aggregates in amyloid-β peptide Aβ40 (*48*). Thus, although the fibrillar state of the rearranged aS variants may still be lower in free energy than the monomeric or unspecifically aggregated states, finding an avenue to the fibrillar state appears to be inefficient. This is analogous to the fact that even nonamyloidogenic β-synuclein can be forced to fibrillize under sufficiently persuasive conditions (*49*), and perhaps this applies to most proteins.

Molecular dynamics simulations suggested that hydrophobic clustering precedes β-sheet formation in the fibrillar misfolding

pathway (*50*). Regions of high, continuous hydrophobicity may therefore favor fibrillization, and their fragmentation may contribute to the absence thereof. Indeed, aS sequence regions of elevated hydrophobicity generally correlate well with regions of high β-sheet propensity (Figure 2A and Figure S5 of the Supporting Information). However, fibrillization can also be suppressed despite the presence of a large hydrophobic cluster, and fibrillization can be maintained despite the elimination of such a cluster. The SaS-C variant created the longest consecutive hydrophobic sequence among all studied variants, including wild-type aS (Figure S5 of the Supporting Information), but nevertheless failed to fibrillize. The deletion mutant aS(Δ73−83), which does not introduce new gaps between β-sheets, eliminates an extended hydrophobic region in the NAC region (Figure S6C of the Supporting Information) but still fibrillizes, albeit not as well as wild-type aS (*22*). In other words, aS(Δ73−83) still allows successful β-sheet pairings, further illustrating redundancy and promiscuity in such pairings. Thus, hydrophobicity plays an important role in fibrillogenesis, but the distribution of β-sheet sequence appears decisive in the case of aS. Similarly, the distribution of charged residues (Figures S5 and S6 of the Supporting Information) will be able to modulate fibrillization kinetics.

By analyzing the fibrillization kinetics and morphologies of four disulfide-restricted aS variants, enclosing the β-sheet propensities of the β3−β4 motif (Figures 1A and 2A), we further demonstrate that a successful protofibril-to-fibril transition is dependent on the accessible range of spatial β-sheet arrangements (Figure 7). It is noteworthy that the aS fibrillization pathway can be dissected in a manner that preserves the efficient formation of protofibrils but selectively prevents fibril formation. Further examples of such behavior are deletion mutants aS(Δ71−82), aS(Δ74−79), and aS(Δ76−77) (*51*, *52*), which involve residues of sheet β4 (Figure 1A) and therefore cannot fibrillize in the canonical cross-β-sheet arrangement of the wild type (Figure 5A). These sequence deletions are in the proximity of the disulfide pairings between sheet β3 and the β4−β5 connector made in this study (Figures 2A and 5A), attesting to the importance of the spatial β3−β4 arrangement in fibril assembly. In this context, we also note the ability of a 9−42 and 69−89 double-disulfide-restricted aS variant to fibrillize (*43*). These residue pairings contain different and more intervening residues than were enclosed by the restrictions made here, which, in turn, may permit larger deviations from the canonical fibril structure of the wild type.

Two additional disulfide-restricted aS variants were studied. The aS(11−26) variant fibrillized, but did so slowly. This is yet another example of a sequence alteration outside of the fibril core that can disturb fibrillization (*21*, *25*). Since aS(11−26) accumulates mainly as amorphous aggregates (Figure 5B), the disulfide restriction appeared to be capable of biasing the structural ensemble in a manner that complicated early β-sheet interactions (Figure 7). The strong preference of several aggregation-inhibiting small molecules for interacting with the region encompassing residues 3−18 and 38−51 is noted in this context (*34*, *53*). Beyond the amphiphilic nature of many aggregation-inhibiting molecules (*34*), the often multivalent character of these molecules, which are also capable of forming micellar aggregates that bias aS conformers but do not induce folding (*34*, *54*), may aid in hindering fibril assembly by restricting the range of accessible β-sheet arrangements. Such a mechanism would be supported by their ability to largely inhibit fibrillization, but not oligomerization (*40*). Finally, the rapid fibrillization kinetics of the intermolecular aS(11)−aS(11) dimer provided further strong evidence that access to the fibrillization pathway is kinetically controlled. In other words, a conformational search underlies aS amyloid misfolding, and the aS(11)−aS(11) disulfide linkage accelerates the sampling of intermolecular interactions.

In summary, the fibrillization kinetics of the 10 aS variants examined in this study indicate that a conformational search underlies the emergence of a first fibrillar aS species. The search efficiency for such a fibril nucleus is sensitive to gaps in sequence between β-sheet regions and the accessible range of spatial β-sheet arrangements at the protofibril stage. On the basis of the universal cross-β-sheet structure of amyloid fibrils (*4*, *7*, *8*), these principles are also expected to apply to the fibrillogenesis of other amyloidogenic proteins. However, highly Asn/Gln-enriched proteins, whose fibrillization strongly depends on the content of these amino acids (*55*), may represent a notable exception to this statement. A relatively inefficient but sequence tolerant search-driven folding pathway may have contributed to the formation of early proteinaceous biomolecules such as amyloids (*9*).

ACKNOWLEDGMENT

We thank Diana Gegala for critically reading the manuscript. We are indebted to Christine Jao and Mario Isas for providing several cysteine mutant aS expression vectors and technical advice. The diligent service of the Scripps Center for Mass Spectrometry (La Jolla, CA) is gratefully acknowledged.

SUPPORTING INFORMATION AVAILABLE

A figure showing the sequence alignment of aS with SaS-A−E, a figure illustrating gel filtration and SDS−PAGE of disulfide-linked aS variants, a figure showing the absence of (proto)fibrillar aggregates following 100 kDa cutoff filtering of aS, a figure comparing the fibrillization kinetics of wild-type aS using proteins of different ages, a figure depicting the distribution of charge and hydrophobicity along the aS and SaS sequences, and a figure comparing β-sheet propensity, charge, and hydrophobicity for aS, SaS-A, and aS(Δ73−83). This material is available free of charge via the Internet at http://pubs.acs.org.

REFERENCES

1. Alzheimer, A. (1907) On a strange disease of the cerebral cortex (translated from German). *Allg. Z. Psychiatr. Ihre Grenzgeb. 64*, 146–148.
2. Lewy, F. H. (1912) Shaking Palsy (translated from Latin). In Pathologische Anatomie. Handbuch der Neurologie (Lewandowsky, M., Ed.) pp 920−933, Springer-Verlag, Berlin.
3. Goedert, M. (2001) α-Synuclein and neurodegenerative diseases. *Nat. Rev. Neurosci. 2*, 492–501.
4. Chiti, F., and Dobson, C. M. (2006) Protein misfolding, functional amyloid, and human disease. *Annu. Rev. Biochem. 75*, 333–366.
5. Lee, V. M. Y., and Trojanowski, J. Q. (2006) Mechanisms of Parkinson's disease linked to pathological α-synuclein: New targets for drug discovery. *Neuron 52*, 33–38.
6. Glabe, C. G. (2006) Common mechanisms of amyloid oligomer pathogenesis in degenerative disease. *Neurobiol. Aging 27*, 570–575.
7. Lashuel, H. A., and Lansbury, P. T. (2006) Are amyloid diseases caused by protein aggregates that mimic bacterial pore-forming toxins? *Q. Rev. Biophys. 39*, 167–201.
8. Tycko, R. (2006) Molecular structure of amyloid fibrils: Insights from solid-state NMR. *Q. Rev. Biophys. 39*, 1–55.
9. Maury, C. P. J. (2009) Self-Propagating β-Sheet Polypeptide Structures as Prebiotic Informational Molecular Entities: The Amyloid World. *Origins Life Evol. Biosphere 39*, 141–150.
10. Shults, C. W. (2006) Lewy bodies. *Proc. Natl. Acad. Sci. U.S.A. 103*, 1661–1668.
11. Davidson, W. S., Jonas, A., Clayton, D. F., and George, J. M. (1998) Stabilization of α-synuclein secondary structure upon binding to synthetic membranes. *J. Biol. Chem. 273*, 9443–9449.

12. Jensen, P. H., Nielsen, M. S., Jakes, R., Dotti, G., and Goedert, M. (1998) Binding of α-synuclein to brain vesicles is abolished by familial Parkinson's disease mutation. *J. Biol. Chem. 273*, 26292–26294.
13. Abeliovich, A., Schmitz, Y., Farinas, I., Choi-Lundberg, D., Ho, W. H., Castillo, P. E., Shinsky, N., Verdugo, J. M. G., Armanini, M., Ryan, A., Hynes, M., Phillips, H., Sulzer, D., and Rosenthal, A. (2000) Mice lacking α-synuclein display functional deficits in the nigrostriatal dopamine system. *Neuron 25*, 239–252.
14. Chen, M., Margittai, M., Chen, J., and Langen, R. (2007) Investigation of α-synuclein fibril structure by site-directed spin labeling. *J. Biol. Chem. 282*, 24970–24979.
15. Vilar, M., Chou, H. T., Luhrs, T., Maji, S. K., Riek-Loher, D., Verel, R., Manning, G., Stahlberg, H., and Riek, R. (2008) The fold of α-synuclein fibrils. *Proc. Natl. Acad. Sci. U.S.A. 105*, 8637–8642.
16. Qin, Z., Hu, D., Han, S., Hong, D. P., and Fink, A. L. (2007) Role of different regions of α-synuclein in the assembly of fibrils. *Biochemistry 46*, 13322–13330.
17. Heise, H., Hoyer, W., Becker, S., Andronesi, O. C., Riedel, D., and Baldus, M. (2005) Molecular-level secondary structure, polymorphism, and dynamics of full-length α-synuclein fibrils studied by solid-state NMR. *Proc. Natl. Acad. Sci. U.S.A. 102*, 15871–15876.
18. Uversky, V. N., Gillespie, J. R., and Fink, A. L. (2000) Why are "natively unfolded" proteins unstructured under physiologic conditions? *Proteins 41*, 415–427.
19. Ueda, K., Fukushima, H., Masliah, E., Xia, Y., Iwai, A., Yoshimoto, M., Otero, D. A. C., Kondo, J., Ihara, Y., and Saitoh, T. (1993) Molecular-Cloning of cDNA Encoding an Unrecognized Component of Amyloid in Alzheimer's Disease. *Proc. Natl. Acad. Sci. U.S.A. 90*, 11282–11286.
20. Han, H. Y., Weinreb, P. H., and Lansbury, P. T. (1995) The Core Alzheimer's Peptide NAC Forms Amyloid Fibrils Which Seed and Are Seeded by β-Amyloid: Is NAC a Common Trigger or Target in Neurodegenerative Disease. *Chem. Biol. 2*, 163–169.
21. Kessler, J. C., Rochet, J. C., and Lansbury, P. T. (2003) The N-terminal repeat domain of α-synuclein inhibits β-sheet and amyloid fibril formation. *Biochemistry 42*, 672–678.
22. Zibaee, S., Jakes, R., Fraser, G., Serpell, L. C., Crowther, R. A., and Goedert, M. (2007) Sequence determinants for amyloid fibrillogenesis of human α-synuclein. *J. Mol. Biol. 374*, 454–464.
23. Murray, I. V. J., Giasson, B. I., Quinn, S. M., Koppaka, V., Axelsen, P. H., Ischiropoulos, H., Trojanowski, J. Q., and Lee, V. M. Y. (2003) Role of α-synuclein carboxy-terminus on fibril formation in vitro. *Biochemistry 42*, 8530–8540.
24. Bertoncini, C. W., Jung, Y. S., Fernandez, C. O., Hoyer, W., Griesinger, C., Jovin, T. M., and Zweckstetter, M. (2005) Release of long-range tertiary interactions potentiates aggregation of natively unstructured α-synuclein. *Proc. Natl. Acad. Sci. U.S.A. 102*, 1430–1435.
25. Ulrih, N. P., Barry, C. H., and Fink, A. L. (2008) Impact of Tyr to Ala mutations on α-synuclein fibrillation and structural properties. *Biochim. Biophys. Acta 1782*, 581–585.
26. Chiti, F., Stefani, M., Taddei, N., Ramponi, G., and Dobson, C. M. (2003) Rationalization of the effects of mutations on peptide and protein aggregation rates. *Nature 424*, 805–808.
27. Thompson, M. J., Sievers, S. A., Karanicolas, J., Ivanova, M. I., Baker, D., and Eisenberg, D. (2006) The 3D profile method for identifying fibril-forming segments of proteins. *Proc. Natl. Acad. Sci. U.S.A. 103*, 4074–4078.
28. Bryan, A. W., Menke, M., Cowen, L. J., Lindquist, S. L., and Berger, B. (2009) BETASCAN: Probable β-amyloids Identified by Pairwise Probabilistic Analysis. *PLoS Comput. Biol. 5*, 1–11.
29. Zibaee, S., Makin, O. S., Goedert, M., and Serpell, L. C. (2007) A simple algorithm locates β-strands in the amyloid fibril core of α-synuclein, Aβ, and tau using the amino acid sequence alone. *Protein Sci. 16*, 906–918.
30. Tartaglia, G. G., and Vendruscolo, M. (2008) The Zyggregator method for predicting protein aggregation propensities. *Chem. Soc. Rev. 37*, 1395–1401.
31. Fernandez-Escamilla, A. M., Rousseau, F., Schymkowitz, J., and Serrano, L. (2004) Prediction of sequence-dependent and mutational effects on the aggregation of peptides and proteins. *Nat. Biotechnol. 22*, 1302–1306.
32. Rao, J. N., Kim, Y. E., Park, L. S., and Ulmer, T. S. (2009) Effect of Pseudorepeat Rearrangement on α-Synuclein Misfolding, Vesicle Binding, and Micelle Binding. *J. Mol. Biol. 390*, 516–529.
33. Hoover, D. M., and Lubkowski, J. (2002) DNAWorks: An automated method for designing oligonucleotides for PCR-based gene synthesis. *Nucleic Acids Res. 30*, No. e43.
34. Rao, J. N., Dua, V., and Ulmer, T. S. (2008) Characterization of α-Synuclein Interactions with Selected Aggregation-Inhibiting Small Molecules. *Biochemistry 47*, 4651–4656.
35. Naiki, H., Higuchi, K., Hosokawa, M., and Takeda, T. (1989) Fluorometric Determination of Amyloid Fibrils in Vitro Using the Fluorescent Dye, Thioflavine-T. *Anal. Biochem. 177*, 244–249.
36. Khurana, R., Coleman, C., Ionescu-Zanetti, C., Carter, S. A., Krishna, V., Grover, R. K., Roy, R., and Singh, S. (2005) Mechanism of thioflavin T binding to amyloid fibrils. *J. Struct. Biol. 151*, 229–238.
37. Wood, S. J., Wypych, J., Steavenson, S., Louis, J. C., Citron, M., and Biere, A. L. (1999) α-Synuclein fibrillogenesis is nucleation-dependent: Implications for the pathogenesis of Parkinson's disease. *J. Biol. Chem. 274*, 19509–19512.
38. Uversky, V. N., Li, J., Souillac, P., Millett, I. S., Doniach, S., Jakes, R., Goedert, M., and Fink, A. L. (2002) Biophysical properties of the synucleins and their propensities to fibrillate: Inhibition of α-synuclein assembly by β- and γ-synucleins. *J. Biol. Chem. 277*, 11970–11978.
39. Park, J. Y., and Lansbury, P. T. (2003) β-Synuclein inhibits formation of α-synuclein protofibrils: A possible therapeutic strategy against Parkinson's disease. *Biochemistry 42*, 3696–3700.
40. Masuda, M., Suzuki, N., Taniguchi, S., Oikawa, T., Nonaka, T., Iwatsubo, T., Hisanaga, S., Goedert, M., and Hasegawa, M. (2006) Small molecule inhibitors of α-synuclein filament assembly. *Biochemistry 45*, 6085–6094.
41. Eliezer, D., Kutluay, E., Bussell, R., and Browne, G. (2001) Conformational properties of α-synuclein in its free and lipid-associated states. *J. Mol. Biol. 307*, 1061–1073.
42. Bernado, P., Bertoncini, C. W., Griesinger, C., Zweckstetter, M., and Blackledge, M. (2005) Defining long-range order and local disorder in native α-synuclein using residual dipolar couplings. *J. Am. Chem. Soc. 127*, 17968–17969.
43. Jiang, C. T., and Chang, J. Y. (2007) Isomers of human α-synuclein stabilized by disulfide bonds exhibit distinct structural and aggregative properties. *Biochemistry 46*, 602–609.
44. Sreerama, N., and Woody, R. W. (2004) Computation and analysis of protein circular dichroism spectra. In Numerical Computer Methods, Part D, pp 318−351, Academic Press Inc., San Diego.
45. Heise, H., Celej, M. S., Becker, S., Riede, D., Pelah, A., Kumar, A., Jovin, T. M., and Baldus, M. (2008) Solid-state NMR reveals structural differences between fibrils of wild-type and disease-related A53T mutant α-synuclein. *J. Mol. Biol. 380*, 444–450.
46. Hoyer, W., Antony, T., Cherny, D., Heim, G., Jovin, T. M., and Subramaniam, V. (2002) Dependence of α-synuclein aggregate morphology on solution conditions. *J. Mol. Biol. 322*, 383–393.
47. Uversky, V. N., Li, J., and Fink, A. L. (2001) Evidence for a partially folded intermediate in α-synuclein fibril formation. *J. Biol. Chem. 276*, 10737–10744.
48. Huang, T. H. J., Yang, D. S., Fraser, P. E., and Chakrabartty, A. (2000) Alternate aggregation pathways of the Alzheimer β-amyloid peptide: An in vitro model of preamyloid. *J. Biol. Chem. 275*, 36436–36440.
49. Yamin, G., Munishkina, L. A., Karymov, M. A., Lyubchenko, Y. L., Uversky, V. N., and Fink, A. L. (2005) Forcing nonamyloidogenic β-synuclein to fibrillate. *Biochemistry 44*, 9096–9107.
50. Hwang, W., Zhang, S. G., Kamm, R. D., and Karplus, M. (2004) Kinetic control of dimer structure formation in amyloid fibrillogenesis. *Proc. Natl. Acad. Sci. U.S.A. 101*, 12916–12921.
51. Giasson, B. I., Murray, I. V. J., Trojanowski, J. Q., and Lee, V. M. Y. (2001) A hydrophobic stretch of 12 amino acid residues in the middle of α-synuclein is essential for filament assembly. *J. Biol. Chem. 276*, 2380–2386.
52. Waxman, E. A., Mazzulli, J. R., and Giasson, B. I. (2009) Characterization of Hydrophobic Residue Requirements for a-Synuclein Fibrillization. *Biochemistry 48*, 9427–9436.
53. Lee, E. N., Cho, H. J., Lee, C. H., Lee, D., Chung, K. C., and Paik, S. R. (2004) Phthalocyanine tetrasulfonates affect the amyloid formation and cytotoxicity of α-synuclein. *Biochemistry 43*, 3704–3715.
54. Stopa, B., Piekarska, B., Konieczny, L., Rybarska, J., Spolnik, P., Zemanek, G., Roterman, I., and Krol, M. (2003) The structure and protein binding of amyloid-specific dye reagents. *Acta Biochim. Pol. 50*, 1213–1227.
55. Ross, E. D., Edskes, H. K., Terry, M. J., and Wickner, R. B. (2005) Primary sequence independence for prion formation. *Proc. Natl. Acad. Sci. U.S.A. 102*, 12825–12830.
56. Clamp, M., Cuff, J., Searle, S. M., and Barton, G. J. (2004) The Jalview Java alignment editor. *Bioinformatics 20*, 426–427.
57. Kyte, J., and Doolittle, R. F. (1982) A Simple Method for Displaying the Hydropathic Character of a Protein. *J. Mol. Biol. 157*, 105.
58. Chou, P. Y., and Fasman, G. D. (1978) Empirical Predictions of Protein Conformation. *Annu. Rev. Biochem. 47*, 251–276.